Front. Phys. 12(3), 127205 (2017)
DOI 10.1007/s11467-016-0636-8

REVIEW ARTICLE

Negative magnetoresistance in Weyl semimetals NbAs and NbP: Intrinsic chiral anomaly and extrinsic effects

Yupeng Li[1], Zhen Wang[1,2], Pengshan Li[3], Xiaojun Yang[1,2], Zhixuan Shen[1], Feng Sheng[1], Xiaodong Li[3], Yunhao Lu[2], Yi Zheng[1,4,5,*], Zhu-An Xu[1,2,4,5,†]

[1] *Department of Physics, Zhejiang University, Hangzhou 310027, China*
[2] *State Key Lab of Silicon Materials, Zhejiang University, Hangzhou 310027, China*
[3] *Institute of High Energy Physics, Chinese Academy of Sciences, Beijing 100049, China*
[4] *Zhejiang California International NanoSystems Institute, Zhejiang University, Hangzhou 310058, China*
[5] *Collaborative Innovation Centre of Advanced Microstructures, Nanjing 210093, China*
*Corresponding authors. E-mail: *phyzhengyi@zju.edu.cn, †zhuan@zju.edu.cn*
Received August 22, 2016; accepted October 9, 2016

Chiral anomaly-induced negative magnetoresistance (NMR) has been widely used as critical transport evidence for the existence of Weyl fermions in topological semimetals. In this mini-review, we discuss the general observation of NMR phenomena in non-centrosymmetric NbP and NbAs. We show that NMR can arise from the intrinsic chiral anomaly of Weyl fermions and/or extrinsic effects, such as the superimposition of Hall signals; field-dependent inhomogeneous current flow in the bulk, i.e., current jetting; and weak localization (WL) of coexistent trivial carriers. The WL-controlled NMR is heavily dependent on sample quality and is characterized by a pronounced crossover from positive to negative MR growth at elevated temperatures, resulting from the competition between the phase coherence time and the spin-orbital scattering constant of the bulk trivial pockets. Thus, the correlation between the NMR and the chiral anomaly need to be scrutinized without the support of complimentary techniques. Because of the lifting of spin degeneracy, the spin orientations of Weyl fermions are either parallel or antiparallel to the momentum, which is a unique physical property known as helicity. The conservation of helicity provides strong protection for the transport of Weyl fermions, which can only be effectively scattered by magnetic impurities. Chemical doping with magnetic and non-magnetic impurities is thus more convincing than the NMR method for detecting the existence of Weyl fermions.

Keywords Weyl semimetals, chiral anomaly, negative magnetoresistance, extrinsic effects

PACS numbers 71.70.Ej, 72.15.Rn, 75.47.-m, 78.40.Kc

Contents

1 Introduction

Quasi-particle excitations of massless Dirac fermions in solids were first proposed in graphene by Wallace in 1947 [1], and the idea of spin non-degenerated Weyl fermions was published even earlier by Weyl in 1929 [2]. However, the experimental exploration of relativistic fermions in solids remained a niche field until the discov-

*Special Topic: Recent Progress on Weyl Semimetals (Eds. Xincheng Xie, Xian-Gang Wan, Hong-Ming Weng & Hua Jiang). arXiv: 1612.04031.

ery of anomalous quantum Hall effects of Dirac fermions in graphene [3, 4]. The birth of topological insulators [5, 6] has triggered intensive competition in the search for new topological semimetals (TSMs), such as Dirac semimetals (DSMs), Dirac nodal-line semimetals, and Weyl semimetals (WSMs) [7–13]. These materials not only host massless fermions, which are the condensed-matter-physics realizations of the long-sought relativistic fermions in high-energy physics, but also exhibit extraordinary physical properties for potential device applications. In general, three-dimensional (3D) DSMs with four-degenerate Dirac nodes near the Fermi level can lift the spin degeneracy of energy bands and transform into 3D Weyl semimetals, by breaking either time-reversal symmetry (TRS) or inversion symmetry (IS) [14]. The latter has been theoretically predicted [11, 12] and experimentally confirmed [15, 16] in the non-magnetic, IS-broken TaAs family, which is widely considered as a major breakthrough in TSMs.

Unlike their magnetic counterpart of pyrochlore iridates [10], WSM states in the TaAs family can be directly detected by angle-resolved photoemission spectroscopy (ARPES), as evident by the existence of Weyl node pairs and linearly dispersed WSM bands [15–18]. WSMs also host symmetry-protected topological surface states. The bulk Weyl nodes with opposite chirality of $\chi = +1$ and $\chi = -1$ are the source and drain points of Berry flux in the momentum space, respectively. The projections of these paired singularities on any surface must be connected by open Fermi arcs [10, 11], which have also been visualized by ARPES. The transport signatures of WSM states [19–22] have been reported simultaneously with the spectroscopy results. However, WSMs share some common features with DSMs [9, 23] in the transport measurements [24]. For example, NbP shows one of the highest records of extremely large magnetoresistance (XMR), which is quasi-linear and non-saturating up to 30 Tesla [21, 22]. Similar XMR was also reported in DSM of Cd_3As_2 [9, 23]. By measuring Shubnikov–de Haas (SdH) oscillations, a nontrivial Berry's phase of π is expected for Weyl fermions, but such a quantum geometrical phase is general for all quasiparticles associated with the massless linear spectrum [25]. In the ultra-quantum regime of strong magnetic field and very low temperature, which was first considered by Nielsen and Ninomiya, two Weyl nodes with opposite chirality can exchange particles when the Fermi level lies within the zeroth Landau level. This effect, which is well known as the Adler–Bell–Jackiw anomaly or the chiral anomaly [26], manifests as negative magnetoresistance (NMR) when the external field is collinear with the applied electric field ($B//E$), as illustrated in Fig. 1(a).

However, anomalous NMR phenomena have been widely observed in the transport measurements of DSMs, such as Cd_3As_2 [9], Na_3Bi [27], $Bi_{1-x}Sb_x$ [28], and $ZrTe_5$ [29], along with the transport reports of chiral anomaly in the TaAs-family WSMs [20, 22, 30, 31]. This raises the question of whether such NMR arises from the intrinsic chiral anomaly or extrinsic factors. One attempt to reconcile the discrepancy between the theoretical prediction and experimental observations was made by Kim *et al.* who proposed that DSMs may transform into WSMs because of the lifting of spin degeneracy by the external magnetic field [28], as illustrated in Fig. 1(b). A similar idea has also been adopted by Hirschberger

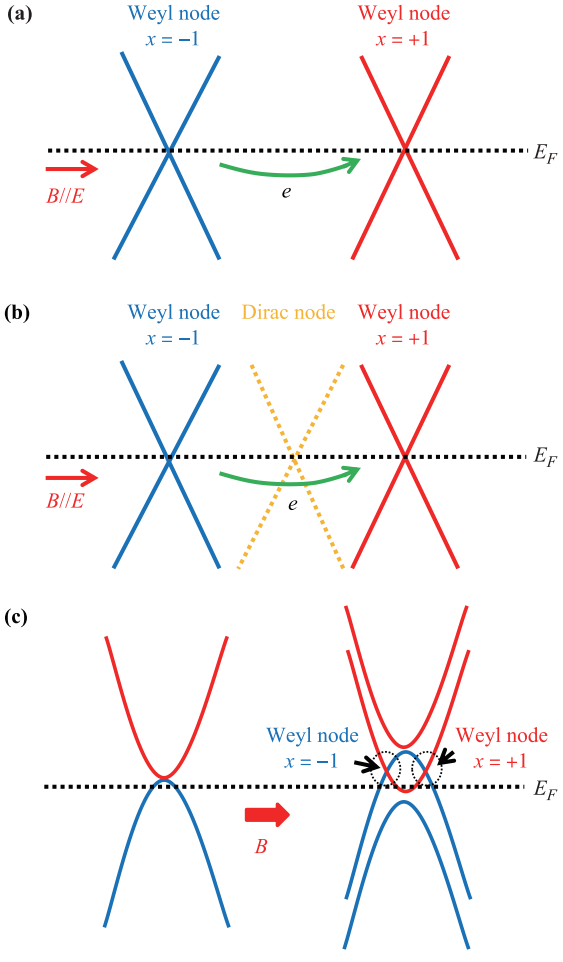

Fig. 1 Semiclassical chiral anomaly in WSMs, DSMs and half-Heusler semiconductors. **(a)** In WSMs, chiral anomaly emerges when B is collinear with E, which creates extra conduction channels between two Weyl nodes with opposite chirality. **(b)** For DSMs, a Dirac cone may split into one pair of Weyl cones in magnetic field, which would explain the observed NMR phenomena. **(c)** Zeeman coupling may also lead to the formation of Weyl nodes in half-Heusler GdPtBi with accidentally touched quadratic bands, each becomes two spin non-degenerate bands in field.

et al. to explain the possible chiral transport in half-Heusler GdPtBi, which is a zero-gap semiconductor with quadratic bands accidentally touching at the Γ point [32].

In real systems, the intrinsic Fermi levels of TaAs-family WSMs are not located exactly at the energy of the chiral nodes. The resulting WSM Fermi surfaces are ellipsoids enclosing the chiral nodes. In such a semi-classical regime, NMR can also arise from the non-zero Berry's curvature, which is satisfied by both DSMs and WSMs [33–35]. The resulting NMR is expected to be quadratic in the weak-field limit [34]. In contrast, the experimental observations of NMR in DSMs and WSMs often extend to the high-field regime, and non-saturating behavior has been reported by different groups [30, 32]. This unusual field dependence, which can surprisingly persist above 100 K, strongly suggests that the current flow in these measured samples is inhomogeneous in the collinear configuration of B and E, a geometrical artifact known as current jetting [36, 37]. Using spot welding to make point-like contacts, dos Reis *et al.* showed that current jetting may play a dominant role in the NMR of the TaAs family [38]. The authors claimed that with $B//E$, the field-dependent resistivity anisotropy ρ_{zz}/ρ_{xx}, which is the ratio of the resistivity (ρ) values perpendicular and parallel to the field direction, can explain all the NMR characteristics reported in the literature [38]. Conversely, Zhang *et al.* suggested that such field-dependent inhomogeneous current distribution can be effectively suppressed by using long and thin bar-shaped samples with electrodes fully crossing the sample width; thus, the intrinsic chiral anomaly-induced NMR can be probed in the low-field regime [39]. However, analytical modeling of the intrinsic chiral anomaly NMR becomes formidable when the specific defect structures of individual samples must be considered. Transmission electron microscope (TEM) has recently revealed that defects are predominantly high-density stacking faults in TaAs, but a mixture of stacking faults, vacancies, and anti-sites in TaP [40].

In this mini-review, we overview our recent studies on the anomalous MR in NbAs and NbP, with a focus on the physical origins of the NMR phenomena with B parallel to E. We elucidate the critical roles of the weak antilocalization (WAL) and weak localization (WL) of bulk trivial carriers in NbAs and NbP, which dominate the anomalous MR in low-quality crystals and at elevated temperatures above 50 K. Unlike massless Weyl fermions, which always produce a steep positive MR in low fields when a Berry's phase of π is accumulated for time-reserved scattering paths, the quantum correction of the trivial pockets is not only field-dependent but also temperature-dependent. Consequently, the trivial-pocket controlled MR is characterized by pronounced crossover behavior from low-field positive growth to NMR, as a result of the competition between the WAL and WL effects. Surprisingly, such crossover behavior is also distinctive above 50 K in high-quality NbP, which has unprecedented charge-carrier mobility of 10^7 cm^2·V^{-1}·s^{-1}, one order of magnitude higher than the other TaAs-family members. This suggests the importance of understanding the defect structures in these binaries. A systematic understanding of NMR and the chiral anomaly will require the preparation of high-quality thin films of the TaAs family to eliminate the inhomogeneous current distribution and to achieve gate-tunable chiral anomaly. For transport experiments, a comparative chemical-doping study of magnetic and non-magnetic impurities provides a more reliable way than NMR of detecting the existence of WSM states. The helicity protection of Weyl fermions in IS-broken WSM can only be invalided by magnetic impurities, as indicated by our recently published results.

2 Discussion

2.1 General NMR characteristics: XMR effect and WAL

We first briefly discuss the band structures of NbP and NbAs, which are noticeably different from the prototype TaAs. In NbP, there exist eight large trivial hole pockets, forming four pairs of inner and outer Fermi surfaces along the S–Z symmetry line [21, 22]. This trivial hole population is compensated by four n-type Weyl fermion pockets in the $k_z = 0$ plane near the high-symmetry points Σ, with each such WSM FS enclosing a trivial electron pocket [22]. In NbAs, compared with NbP, the band top of the trivial hole pockets is closer to the Fermi energy, which effectively reduces the charge-carrier concentration in the binary (Fig. 2). This change mainly comes from the hybridization of the As-4p and Nb-4d orbitals, while the spin-orbital coupling (SOC) magnitude in both systems is comparable with the same transition metal Nb cations.

Due to the broken IS, the energy bands of NbP and NbAs are spin-lifted. Thus, all the charge carriers in these two compounds are spin-polarized, similar to the case in noncentrosymmetric WTe_2 [41]. For WSM pockets enclosing chiral nodes, the spin orientation is either parallel or anti-parallel to the momentum, i.e., helicity, which is rooted in the massless Hamiltonian of WSMs: $\widehat{H} = \mathrm{i}\hbar v_{\mathrm{F}} \boldsymbol{\sigma} \cdot \boldsymbol{K}$. Helicity provides extremely strong protection for the transport of Weyl fermions against the scattering of non-magnetic defects and leads to a spectacular charge-carrier mobility of 1×10^7 cm^2·V^{-1}·s^{-1} at 1.5 K in NbP with a moderate residual-resistivity ratio (RRR) of ~ 100 [22]. For NbAs, we did not observe comparable mobility, which is about $\sim 3 \times 10^5$ cm^2·V^{-1}·s^{-1}

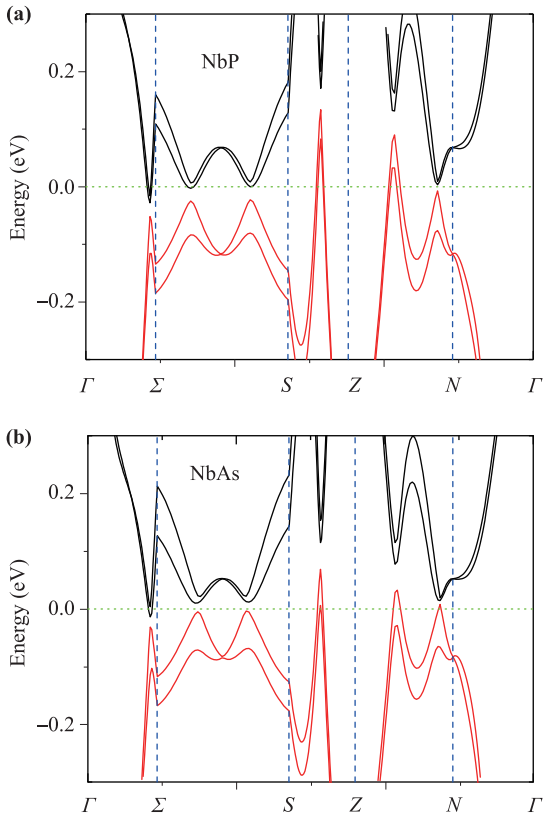

Fig. 2 The energy band structures of NbP **(a)** and NbAs **(b)**. The change from P-3p to As-4p orbitals effectively reduces the trivial hole-pocket size and the overall charge carrier density.

for high-quality crystals with RRR of $\sim$ 100. Distinctively, the anomalous MR of the NbAs samples with $B//E$ shows a steep MR upturn in low magnetic field, which is generally observed for TaAs [39] and TaP [30] at the helium temperature but nearly indistinguishable in NbP [22].

One possible contribution of this low-field MR hump is the XMR effect induced by a small misaligned angle between B and E. In our experiments, we adopted a different angle-rotation configuration from that in the literature, as shown in Fig. 3, in which E is along the b-axis and B is rotated in the a–b plane. The zero degree is defined as the minimum point of the averaged MR versus angle curve for $B = \pm 3$ T, respectively, measured by a rotation step of 0.5°. As shown in Fig. 3, at the presumptive 0°, the anomalous MR in NbAs is characterized by a low-field resistance hump, followed by the intermediate-field NMR growth. Above 3 T, the MR curve resumes slow positive growth, an indication of the good angle alignment by our method. As a comparison, we plotted sin5° of the transverse MR (90°, for $I//b$, and $B//a$) as the pink dashed line in Fig. 3, which would represents an extreme case of poor B and E alignment. It is clear that the experimental low-field positive MR grows faster than the parabolic-like curve, which demonstrates that the low-field MR cannot be simply explained by the coupling of the XMR effect.

It is intriguing that the steep MR upturn is also sample quality dependent. Figure 4 shows the angle-dependent MR curves in the vicinity of 0° for a high-quality sample with RRR exceeding 130 (NbAs-S12), in contrast to RRR $\approx$ 8 for the sample shown in Fig. 3 (NbAs-S4). Despite that the overall MR characteristics are highly sensitive to the rotation angle (θ), the low-field parts are nearly identical between $\pm$0.2 T. Above 0.2 T, the dwindling of the XMR contribution to the anomalous NMR in NbAs is evident when θ changes from −4.2° to −0.2°. The nominal 0° MR curve surprisingly shows a weaker field dependence in NMR growth, which deviates from

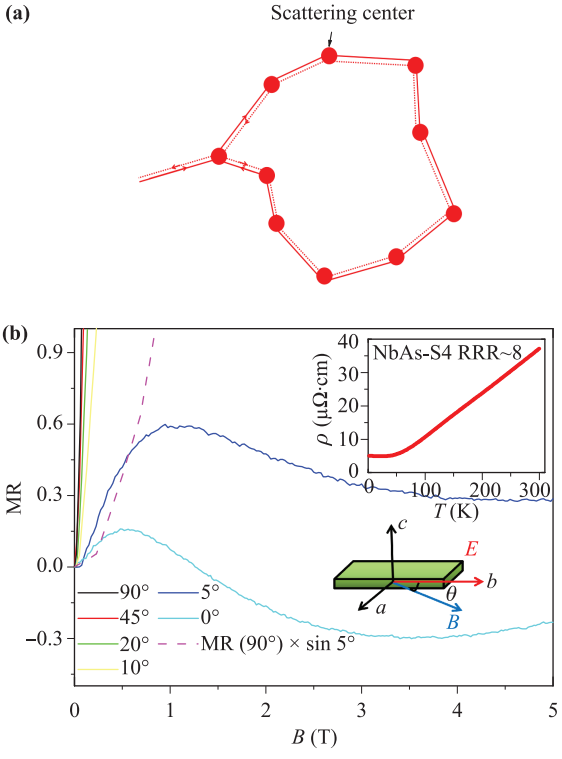

Fig. 3 **(a)** Schematic of quantum interference induced by time reversed scattering paths. **(b)** Angle-dependent anomalous MR in low-quality NbAs-S4. The pink dashed line is calculated from the transverse MR at 90°, by assuming a large B and E misalignment of 5°. Inset: Sample geometry: Single crystals of NbAs and NbP are polished into long and thin bar-shaped slabs with current contacts fully covering both long ends. The voltage leads are not point contacts on the top surface of the slab, but crossing the whole side surface along the c-axis to minimize the current jetting effect. Note that E and B are in the same plane during the angle rotation, and a- and b-axis are equivalent due to the lattice symmetry.

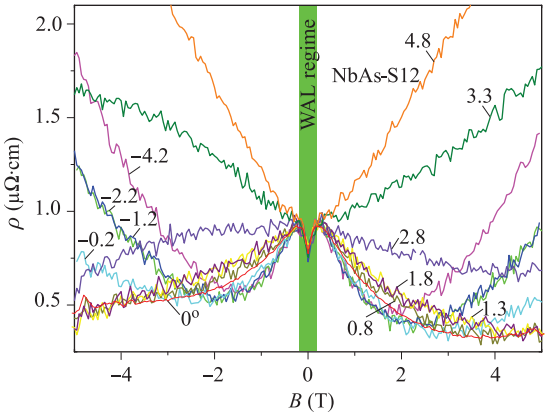

Fig. 4 Angle-dependent anomalous MR in high-quality NbAs-S12, in the vicinity of $B//E$. The definition of the nominal 0° is explained in the main texts. Distinctively, the steep low-field MR hump is independent of angle rotations.

$1/B^2$ and extends to substantially higher fields compared with the negative angles. Further increase in θ gradually weakens the field dependence of NMR, which becomes non-saturating at 1.3°, 1.8°, and 2.8°. At angles lager than 3.3°, NMR is completely absent, and positive MR growth dominates above 0.2 T.

Although these experimental results can be interpreted in various ways, as proposed in the literature [30, 38, 39], the θ-independent growth suggests that the low-field MR is not dominated by the XMR effect or current jetting, both are sensitive to the alignment of B and E. With the presence of massless Weyl fermions and spin-polarized trivial carriers, quantum inference-induced MR correction is expected. Such a quantum effect is illustrated in Fig. 3(a), which shows a closed scattering trajectory (the solid line) and its time-reversed path (the dotted line). For Weyl fermions, backscattering along these two time-reversed paths is equivalent to a closed circle movement in the momentum space, which leads to a Berry's phase of π [42]. Consequently, destructive quantum interference, i.e., WAL, is typical for WSM pockets at low temperatures. In contrast, the conservation of the spin-momentum geometry of trivial carriers, which is not well-defined quantum numbers, is determined by the nature of individual scattering events. The resulting quantum correction is a pronounced competition between WAL and WL, which is determined by the spin-orbital scattering time (τ_{SO}) and the phase decoherence time (τ_Φ), respectively. When non-magnetic impurity scattering is dominant, i.e., a very small τ_Φ, the quantum interference is always in-phase and constructive, producing WL correction to MR [43]. On the other hand, if $\tau_\phi \gg \tau_{SO}$, the quantum correction is antiphase, and WAL dominates. In the intermediate regime of $\tau_\phi \approx \tau_{SO}$, there can be a field-dependent transition from WAL to WL [44].

In both the $\tau_\phi \gg \tau_{SO}$ and $\tau_{SO} \gg \tau_\phi$ regimes, the quantum correction to the conductivity with collinear B and E can be formulated by [45]

$$\Delta\sigma(B) \cong \alpha \frac{-e^2}{2\pi^2\hbar} \ln\left(1 + \beta \frac{ed^2}{\hbar B_\Phi} B^2\right), \tag{1}$$

in which $\hbar$ is the Planck's constant, e is the electron charge, d is the sample thickness, B_Φ is the critical field required to dephase the quantum interference, and β is a fitting parameter. The difference between WAL and WL lies in the coefficient α, which is 1/2 for the former and −1 for the latter. For practical purposes, the low-field WAL correction can be simplified as $\sigma_2 + a\sqrt{B}$ [28, 46]. By assuming a parabolic chiral magnetic conductivity of $C_W B^2$ [28, 34], we fit the experimental anomalous MR using an empirical model:

$$\rho(B) = \frac{1}{\sigma_{WAL} \cdot (1 + C_W B^2)} + A_1 B^2 + A_2 B, \tag{2}$$

where σ_0 is the zero-field conductivity, $A_1 B^2$ is the XMR contribution due to θ misalignment, and $A_2 B$ is a linear correction to the resistivity, which includes the contributions of large Hall signals in NbAs or current jetting. The validity of Eq. (2) is justified by the good alignment between B and E, which ensures that the XMR contribution is negligible under weak fields. Indeed, the model captures all the essential features of the anomalous MR, including the low-field MR hump below 0.2 T, followed by the parabolic NMR, and the positive XMR growth above 2 T, as shown in Fig. 5 for the −4.2° data in Fig. 4. However, for 0° and a positive θ, Eq. (2) does

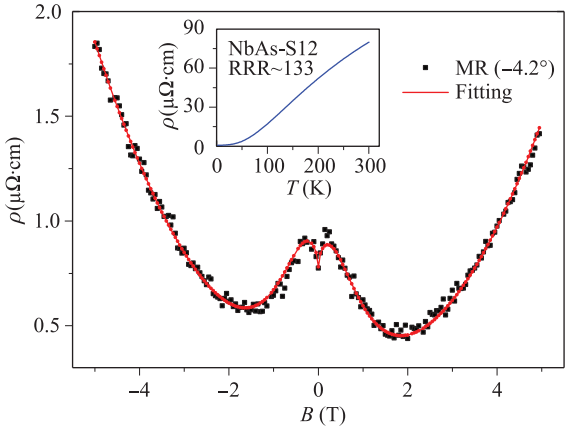

Fig. 5 Fitting of the anomalous MR curve at −4.2° for NbAs-S12, using the Eq. (2) in the main texts. The low-field MR follows the B^2 model, while the intermediate-field NMR growth is inversely proportional to B^2. Note that a linear correction from Hall or current-jetting is superimposed on the anomalous MR characteristics.

not fit the NMR growth, which deviates from $1/(C_W B^2)$ significantly.

For WSM associated WAL, it is also expected to be robust at elevated temperatures, although electron-phonon and intravalley electron-electron interactions will weaken the helicity-protection mechanism. Figure 6 shows the T-dependent MR at the nominal 0° for NbAs-S12. It is clear that NMR has stronger T dependence than the WAL-dominated low-field MR cusp, which is nearly identical below 20 K. At 50 K, NMR disappears completely, while low-field WAL becomes broader in field dependence and is followed by parabolic-like XMR above 2 T. Above 50 K, the anomalous MR is dominated by the XMR effect, which becomes saturating under strong field, as in the case of conventional semimetals [47, 48].

2.2 Non-saturating NMR: Contribution of WL from trivial pockets

Noticeably, sample quality plays a critical role in the T-dependent anomalous MR in NbAs. In Fig. 7, we show the T-dependent MR curves for NbAs-S4, which has an RRR ($\sim$ 8) one order of magnitude lower than that of NbAs-S12. The low-field positive MR cusp in this sample is largely extended to 0.5 T and shows significant T dependence below 20 K. Unlike the high-quality NbAs-S12, there are broad transitions from positive to negative MR in NbAs-S4. At 50 K, the NMR in NbAs-S4 becomes non-saturating up to 5 T. Further increase in T to 100 K, the low-field positive MR becomes parabolic-like, suggesting its origin in the XMR effect. However, above 3 T, negative MR growth gradually takes over. Li *et al.* proposed that this unusual crossover feature is correlated to a pronounced field-dependent competition

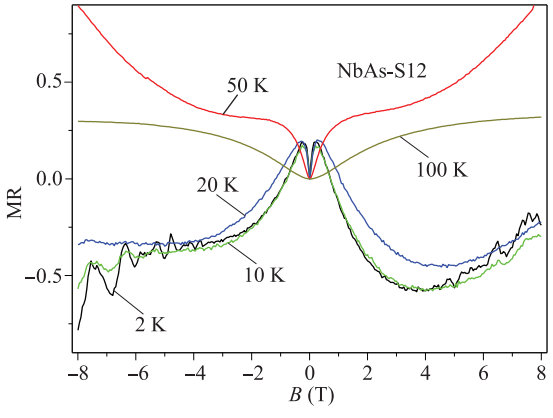

Fig. 6 T-dependent WAL in high-quality NbAs-S12. At 50 K, the MR curve clearly shows the WAL-related positive growth, followed by the parabolic-like XMR effect. Note that NMR is completely suppressed at this temperature. At 100 K, typical XMR behavior is observed, which becomes saturating in high fields.

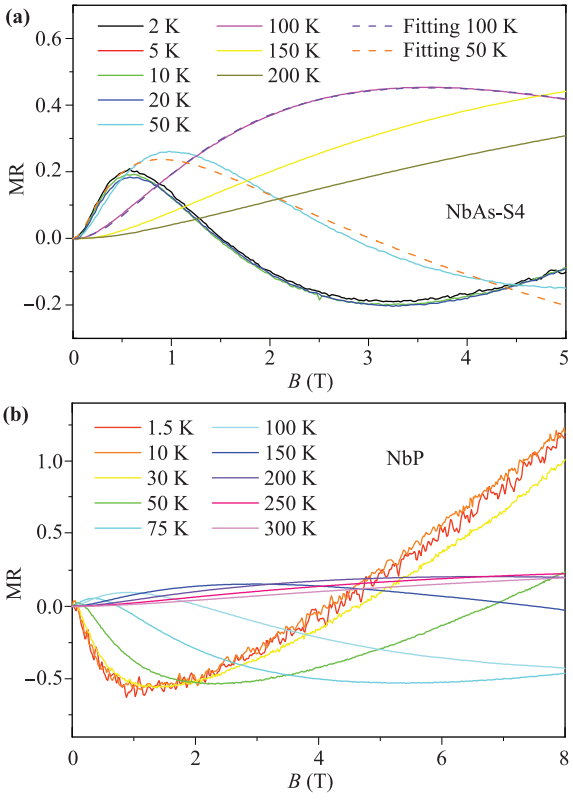

Fig. 7 **(a)** T-dependent anomalous MR in low-quality NbAs-S4. The low-field positive MR is significantly different from the high-quality sample in Fig. 6. **(b)** T-dependent anomalous MR in high-quality, stoichiometric NbP. At helium temperature, the low-field positive MR cusp is nearly indistinguishable. Above 50 K, broad WAL-WL crossover characteristics are dominant. Reproduced from Ref. [22].

between the WAL and WL of trivial bulk pockets [49]. It is noteworthy that the coexistence of nontrivial and trivial pockets is not only reported for the MPn_2 family (M = Nb and Ta; Pn = As and Sb) [49–52], but rather general for topological SMs with strong SOC.

In the regime of $\tau_{SO} \sim \tau_\phi$ [44], such trivial pocket-contributed broad crossover with $B//E$ can be modeled by assuming two independent scattering processes for WAL and WL:

$$\frac{\Delta R}{R_0} = \alpha \left[\frac{1}{2} \ln(1 + bB^2 L_\phi^2) - \frac{3}{2} \ln(1 + bB^2 L_{SO}^2) \right], \quad (3)$$

where $L_{SO} \propto \tau_{SO}$ and $L_\phi \propto \tau_\phi$ are the spin-orbital scattering length and the phase coherent length, respectively. WAL is dominant in low fields when $\tau_\phi > \tau_{SO}$. However, WL gradually takes over in high fields due to a larger coefficient of 3/2 than the 1/2 for WAL. More importantly, τ_{SO} is an intrinsic parameter of SOC in the bulk and is thus weakly dependent on T changes, whereas τ_ϕ is highly sensitive to T. Such distinct T dependence between τ_{SO} and τ_ϕ leads to pronounced T-dependent

crossover characteristics. In Fig. 7, we show the data fitting for 50 and 100 K using Eq. (3). At 100 K, the model provides a satisfying description of the field dependence. In contrast, the fitting for the 50 K data is less successful, which implies the contributions of the chiral anomaly or other extrinsic effects to the NMR.

It should be emphasized here that Eq. (3) is a variation of the Dugaev–Khmelnitskii model [53], which in principle requires $d \ll l$. Here, l is the mean free path of trivial carriers, which is several orders of magnitude smaller than the typical sample thickness (d) of 200 μm in our experiments. The applicability of Eq. (3) to thick NbAs samples may be correlated to the formation of unique stacking-fault defects in the a–b plane, which essentially produces quasi-two dimensional structure of $I4_1md$ lattice sandwiched by hexagonal lattice of $P\bar{6}m2$ [40]. In Fig. 8, we show the typical angle-dispersive X-ray diffraction patterns of a low-quality NbAs single crystal, which clearly shows stacking fault-related streaks. For NbP, highly stoichiometric single crystals can be synthesized, as manifested by the unprecedented charge-carrier mobility of 1×10^7 $cm^2 \cdot V^{-1} \cdot s^{-1}$ [22]. However, we have also observed broad WAL-WL crossover in NbP above 50 K [22], which implies that stacking-fault defects may be universal for the TaAs family.

2.3 Probing Weyl fermions by magnetic impurities

Because the helicity protection of Weyl fermions in the TaAs class relies on intact TRS, comparative chemical

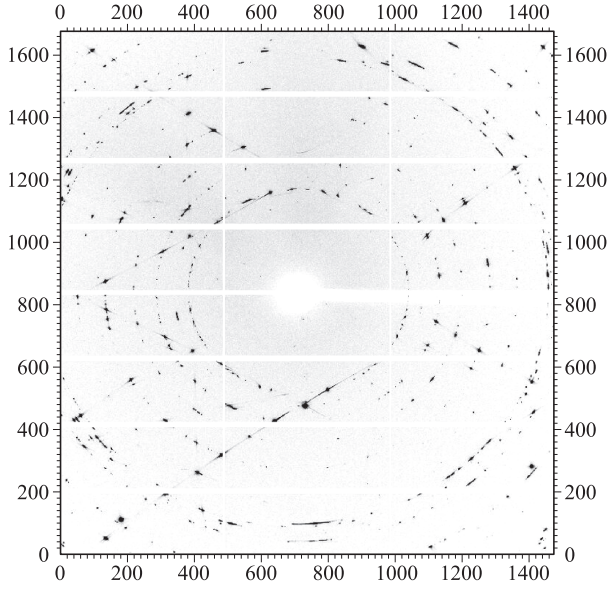

Fig. 8 Angle-dispersive X-ray diffraction of a low quality NbAs single crystal, showing typical diffraction-streaks induced by stacking fault lines. Similar defects have also been reported in TaP and TaAs by scanning TEM [40].

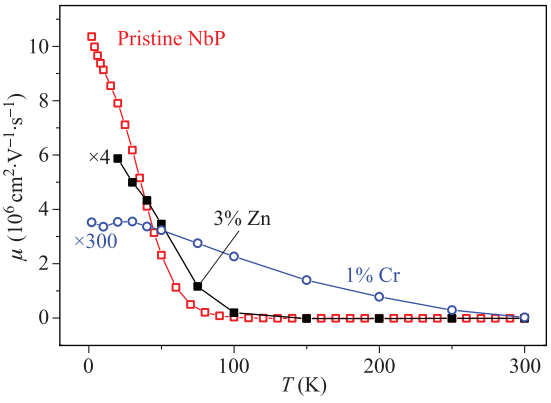

Fig. 9 Magnetic vs. non-magnetic impurities in NbP. The ultrahigh charge-carrier mobility of NbP is degraded by more than two orders of magnitude by ∼ 1% Chromium, but insensitive to Zinc impurities. Reproduced from Ref. [22].

doping of non-magnetic and magnetic impurities in this family provides an indispensable way in probing the existence of Weyl fermions. In our previous study [22], we have shown that a minimal amount of chromium (∼ 1%) in NbP degrades the charge-carrier mobility by more than two orders of magnitude, while three times higher concentration of non-magnetic zinc yields comparable mobility to pristine NbP (see Fig. 9). Compared with the $B//E$ NMR method, which may be completely dominated by extrinsic effects from multiple sources instead of the chiral anomaly, chemical-doping experiments provide effective transport evidence of the existence of WSM states. Equally importantly, the interaction of magnetic impurities with Weyl fermions at low temperatures may lead to novel Kondo physics of massless fermions [54], which has not been experimentally explored.

3 Conclusion

The discovery of WSM states in the IS-broken TaAs class has been a major breakthrough in condensed matter physics. The experimental observations of NMR have been extensively used as a hallmark of WSM states in TaAs and the other three binaries. However, the recent experiments have raised the question of whether NMR can be used as unambiguous transport evidence for the existence of Weyl fermions. Here, we have discussed the general observation of anomalous MR in NbP and NbAs in the configuration of collinear B and E, which is a prerequisite for the chiral anomaly. We have elucidated that the low-field steep positive MR is WAL correlated, but not necessary to be associated with WSM states, whereas the following intermediate-field NMR may arise from the intrinsic chiral anomaly and/or various extrinsic effects. In particular, we highlight the WL contribution

to NMR from trivial pockets in NbAs and NbP, which coexist with WSM states. The trivial pocket-controlled WL is sensitive to crystal quality, and low-RRR samples exhibit more pronounced extrinsic NMR, normally characterized by broad positive-to-negative MR transition behavior and weaker field dependence than the theoretical parabolic magnetoconductance of the chiral anomaly. At elevated temperatures, the WL-contributed NMR becomes predominant and shows non-saturating behavior in field growth, which is expected to be general for topological SMs with strong SOC and coexisting nontrivial and trivial pockets.

Chemical doping of non-magnetic and magnetic impurities provides a more reliable way to probe the existence of WSM states than other methods by detecting the helicity protection mechanism of Weyl fermions. Note that such a method is also valid for other relativistic fermions with spin-momentum locking, such as helical Dirac fermions in Rashiba SMs and TIs. A complete understanding of chiral anomaly induced NMR would be feasible by preparing the TaAs class in thin films using methods such as chemical vapor deposition and pulse laser deposition. With thin-film samples, it will be possible to introduce gate tunability to study Fermi energy-dependent chiral anomaly in this family, which would allow the ultra quantum-limit chiral magnetoconductance to be studied for the first time.

Acknowledgements This work was supported by the National Basic Research Program of China (Grant No. 2014CB921203), the National Science Foundation of China (Grant Nos. 11190023, U1332209, 11374009, 61574123, and 11574264), MOE of China (Grant No. 2015KF07), the Fundamental Research Funds for the Central Universities of China, and the National Key R&D Program of the MOST of China (Grant No. 2016YFA0300204). The in-situ high-pressure angle-dispersive X-ray diffraction (ADXRD) measure- ment was performed at the 4W2 beamline of the Beijing Synchrotron Radiation Facility (BSRF). Y.Z. acknowledges the start funding support from the Thousand Talents Plan.

References

1. P. R. Wallace, The band theory of graphite, *Phys. Rev.* 71(9), 622 (1947)
2. H. Weyl, Elektron und gravitation. I, *Z. Phys.* 56(5–6), 330 (1929)
3. K. S. Novoselov, A. K. Geim, S. V. Morozov, D. Jiang, M. I. Katsnelson, I. V. Grigorieva, S. V. Dubonos, and A. A. Firsov, Two-dimensional gas of massless Dirac fermions in graphene, *Nature* 438(7065), 197 (2005)
4. Y. B. Zhang, Y. W. Tan, H. L. Stormer, and P. Kim, Experimental observation of the quantum Hall effect and Berry's phase in graphene, *Nature* 438(7065), 201 (2005)
5. M. Z. Hasan and C. L. Kane, Colloquium: Topological insulators, *Rev. Mod. Phys.* 82(4), 3045 (2010)
6. X. L. Qi and S. C. Zhang, Topological insulators and superconductors, *Rev. Mod. Phys.* 83(4), 1057 (2011)
7. S. M. Young, S. Zaheer, J. C. Y. Teo, C. L. Kane, E. J. Mele, and A. M. Rappe, Dirac semimetal in three dimensions, *Phys. Rev. Lett.* 108(14), 140405 (2012)
8. Z. Wang, H. Weng, Q. Wu, X. Dai, and Z. Fang, Three-dimensional Dirac semimetal and quantum transport in Cd_3As_2, *Phys. Rev. B* 88(12), 125427 (2013)
9. L. Tian, Q. Gibson, M. N. Ali, M. Liu, R. J. Cava, and N. P. Ong, Ultrahigh mobility and giant magnetoresistance in the Dirac semimetal Cd_3As_2, *Nat. Mater.* 14, 280 (2015)
10. X. G. Wan, A. M. Turner, A. Vishwanath, and S. Y. Savrasov, Topological semimetal and Fermi-arc surface states in the electronic structure of pyrochlore iridates, *Phys. Rev. B* 83(20), 205101 (2011)
11. H. Weng, C. Fang, Z. Fang, B. A. Bernevig, and X. Dai, Weyl semimetal phase in noncentrosymmetric transition-metal monophosphides, *Phys. Rev. X* 5(1), 011029 (2015)
12. S. Huang, S. Y. Xu, I. Belopolski, C. Lee, G. Chang, B. Wang, N. Alidoust, G. Bian, M. Neupane, C. Zhang, S. Jia, A. Bansil, H. Lin, and M. Z. Hasan, A Weyl Fermion semimetal with surface Fermi arcs in the transition metal monopnictide TaAs class, *Nat. Commun.* 6, 7373 (2015)
13. G. Bian, T. R. Chang, R. Sankar, S. Y. Xu, H. Zheng, T. Neupert, C. K. Chiu, S. M. Huang, G. Chang, I. Belopolski, D. S. Sanchez, M. Neupane, N. Alidoust, C. Liu, B.K. Wang, C.-C. Lee, H.-T. Jeng, A. Bansil, F. Chou, H. Lin, and M. Z. Hasan, Topological nodal-line fermions in the non-centrosymmetric superconductor compound $PbTaSe_2$, arXiv: 1505.03069 (2015)
14. G. B. Halász and L. Balents, Time-reversal invariant realization of the Weyl semimetal phase, *Phys. Rev. B* 85(3), 035103 (2012)
15. S.Y. Xu, N. Alidoust, I. Belopolski, Z. Yuan, G. Bian, T.R. Chang, H. Zheng, V. N. Strocov, D. S. Sanchez, G. Chang, C. Zhang, D. Mou, Y. Wu, L. Huang, C.C. Lee, S.M. Huang, B. K. Wang, A. Bansil, H.T. Jeng, T. Neupert, A. Kaminski, H. Lin, S. Jia, and M. Z. Hasan, Discovery of a Weyl fermion state with Fermi arcs in niobium arsenide, *Nat. Phys.* 11(9), 748 (2015)
16. B. Q. Lv, H. M. Weng, B. B. Fu, X. P. Wang, H. Miao, J. Ma, P. Richard, X. C. Huang, L. X. Zhao, G. F. Chen, Z. Fang, X. Dai, T. Qian, and H. Ding, Experimental discovery of Weyl semimetal TaAs, *Phys. Rev. X* 5(3), 031013 (2015)
17. B. Q. Lv, S. Muff, T. Qian, Z. D. Song, S. M. Nie, N. Xu, P. Richard, C. E. Matt, N. C. Plumb, L. X. Zhao, G. F. Chen, Z. Fang, X. Dai, J. H. Dil, J. Mesot, M. Shi, H. M. Weng, and H. Ding, Observation of Fermi-arc spin texture in TaAs, *Phys. Rev. Lett.* 115, 217601 (2015)

18. S. Xu, I. Belopolski, N. Alidoust, M. Neupane, G. Bian, C. Zhang, R. Sankar, G. Chang, Z. Yuan, C. C. Lee, S.M. Huang, H. Zheng, J. Ma, D. S. Sanchez, B. Wang, A. Bansil, F. Chou, P. P. Shibayev, H. Lin, S. Jia, and M. Z. Hasan, Discovery of a Weyl fermion semimetal and topological Fermi arcs, *Science* 349(6248), 613 (2015)

19. C. Zhang, Z. Yuan, S. Xu, Z. Lin, B. Tong, M. Z. Hasan, J. Wang, C. Zhang, and S. Jia, Tantalum monoarsenide: An exotic compensated semimetal, arXiv: 1502.00251 (2015)

20. X. Huang, L. Zhao, Y. Long, P. Wang, D. Chen, Z. Yang, H. Liang, M. Xue, H. M. Weng, Z. Fang, X. Dai, and G. Chen, Observation of the chiral anomaly induced negative magnetoresistance in 3D Weyl semimetal TaAs, *Phys. Rev. X* 5(3), 031023 (2015)

21. C. Shekhar, A. K. Nayak, Y. Sun, M. Schmidt, M. Nicklas, I. Leermakers, U. Zeitler, Y. Skourski, J. Wosnitza, Z. Liu, Y. Chen, W. Schnelle, H. Borrmann, Y. Grin, C. Felser, and B. H. Yan, Extremely large magnetoresistance and ultrahigh mobility in the topological Weyl semimetal candidate NbP, *Nat. Phys.* 11(8), 645 (2015)

22. Z. Wang, Y. Zheng, Z. X. Shen, Y. Zhou, X. J. Yang, Y. P. Li, C. M. Feng, and Z. A. Xu, Helicity protected ultrahigh mobility Weyl fermions in NbP, *Phys. Rev. B* 93, 121112(R) (2016)

23. A. Narayanan, M. D. Watson, S. F. Blake, N. Bruyant, L. Drigo, Y. L. Chen, D. Prabhakaran, B. Yan, C. Felser, T. Kong, P. C. Canfield, and A. I. Coldea, Linear magnetoresistance caused by mobility fluctuations in n-doped Cd_3As_2, *Phys. Rev. Lett.* 114(11), 117201 (2015)

24. P. Hosur and X. L. Qi, Recent developments in transport phenomena in Weyl semimetals, *C. R. Phys.* 14(9–10), 857 (2013)

25. I. A. Luk'yanchuk and Y. Kopelevich, Phase analysis of quantum oscillation in graphite, *Phys. Rev. Lett.* 93(16), 166402 (2004)

26. H. B. Nielsen and M. Ninomiya, The Adler-Bell-Jackiw anomaly and Weyl fermions in a crystal, *Phys. Lett. B* 130(6), 389 (1983)

27. J. Xiong, S. K. Kushwaha, T. Liang, J. W. Krizan, M. Hirschberger, W. Wang, R. J. Cava, and N. P. Ong, Evidence for the chiral anomaly in the Dirac semimetal Na_3Bi, *Science* 350(6259), 413 (2015)

28. H. J. Kim, K. S. Kim, J. F. Wang, M. Sasaki, N. Satoh, A. Ohnishi, M. Kitaura, M. Yang, and L. Li, Dirac versus Weyl fermions in topoogical insulators: Adler–Bell–Jackiw anomaly in transport phenomena, *Phys. Rev. Lett.* 111(24), 246603 (2013)

29. Q. Li, D. E. Kharzeev, C. Zhang, Y. Huang, I. Pletikosic, A. V. Fedorov, R. D. Zhong, J. A. Schneeloch, G. D. Gu, and T. Valla, Observation of the chiral magnetic effect in $ZrTe_5$, arXiv: 1412.6543 (2014)

30. F. Arnold, C. Shekhar, S.-C. Wu, Y. Sun, R. Donizeth dos Reis, N. Kumar, M. Naumann, M. O. Ajeesh, M. Schmidt, A. G. Grushin, J. H. Bardarson, M. Baenitz, D. Sokolov, H. Borrmann, M. Nicklas, C. Felser, E. Hassinger, and B. Yan, Large and unsaturated negative magnetoresistance induced by the chiral anomaly in the Weyl semimetal TaP, arXiv: 1506.06577 (2015)

31. X. J. Yang, Y. P. Li, Z. Wang, Y. Zheng, and Z. A. Xu, Chiral anomaly induced negative magnetoresistance in topological Weyl semimetal NbAs, arXiv: 1506.03190 (2015)

32. M. Hirschberger, S. Kushwaha, Z. Wang, Q. Gibson, S. Liang, C. A. Belvin, B. A. Bernevig, R. J. Cava, and N. P. Ong, The chiral anomaly and thermopower of Weyl fermions in the half-Heusler GdPtBi, Nat. Mater. 15(11), 1161 (2016)

33. D. T. Son and B. Z. Spivak, Chiral anomaly and classical negative magnetoresistance of Weyl metals, *Phys. Rev. B* 88(10), 104412 (2013)

34. A. A. Burkov, Negative longitudinal magnetoresistance in Dirac and Weyl metals, *Phys. Rev. B* 91(24), 245157 (2015)

35. B. Z. Spivak and A. V. Andreev, Magneto-transport phenomena related to the chiral anomaly in Weyl semimetals, *Phys. Rev. B* 93(8), 085107 (2016)

36. J. S. Hu, T. F. Rosenbaum, and J. B. Betts, Current jets, disorder, and linear magnetoresistance in the silver chalcogenides, *Phys. Rev. Lett.* 95(18), 186603 (2005)

37. J. S. Hu, M. M. Parish, and T. F. Rosenbaum, Nonsaturating magnetoresistance of inhomogeneous conductors: Comparison of experiment and simulation, *Phys. Rev. B* 75(21), 214203 (2007)

38. R. D. dos Reis, M. O. Ajeesh, N. Kumar, F. Arnold, C. Shekhar, M. Naumann, M. Schmidt, M. Nicklas, and E. Hassinger, On the search for the chiral anomaly in Weyl semimetals: The negative longitudinal magnetoresistance, arXiv: 1606.03389 (2016)

39. C. L. Zhang, S. Y. Xu, I. Belopolski, Z. Yuan, Z. Lin, B. Tong, G. Bian, N. Alidoust, C. C. Lee, S. M. Huang, T. R. Chang, G. Chang, C. H. Hsu, H. T. Jeng, M. Neupane, D. S. Sanchez, H. Zheng, J. Wang, H. Lin, C. Zhang, H. Z. Lu, S. Q. Shen, T. Neupert, M. Z. Hasan, and S. Jia, Signatures of the Adler–Bell–Jackiw chiral anomaly in a Weyl fermion semimetal, *Nat. Commun.* 7, 10735 (2016)

40. T. Besara, D. A. Rhodes, K. W. Chen, S. Das, Q. R. Zhang, J. F. Sun, B. Zeng, Y. Xin, L. Balicas, R. E. Baumbach, E. Manousakis, D. J. Singh, and T. Siegrist, Coexistence of Weyl physics and planar defects in semimetals TaP and TaAs, *Phys. Rev. B* 93, 245152 (2016), arXiv: 1606.05178

41. J. Jiang, F. Tang, X. C. Pan, H. M. Liu, X. H. Niu, Y. X. Wang, D. F. Xu, H. F. Yang, B. P. Xie, F. Q. Song, P. Dudin, T. K. Kim, M. Hoesch, P. K. Das, I. Vobornik, X. G. Wan, and D. L. Feng, Signature

of strong spin-orbital coupling in the large nonsaturating magnetoresistance material WTe_2, *Phys. Rev. Lett.* 115(16), 166601 (2015)

42. K. Y. Bliokh, Weak antilocalization of ultrarelativistic fermions, *Phys. Lett. A* 344(2–4), 127 (2005)
43. S. Hikami, A. I. Larkin, and Y. Nagaoka, Spin-orbital interaction and magnetoresistance in the two-dimensional random system, *Prog. Theor. Phys.* 63(2), 707 (1980)
44. H. Wang, H. Liu, C. Z. Chang, H. Zuo, Y. Zhao, Y. Sun, Z. Xia, K. He, X. Ma, X. C. Xie, Q. K. Xue, and J. Wang, Crossover between weak antilocalization and weak localization of bulk states in ultrathin Bi_2Se_3 films, *Sci. Rep.* 4, 5817 (2014)
45. C. J. Lin, X. Y. He, J. Liao, X. X. Wang, V. Sacksteder IV, W. M. Yang, T. Guan, Q. M. Zhang, L. Gu, G. Y. Zhang, C. G. Zeng, X. Dai, K. H. Wu, and Y. Q. Li, Parallel field magnetoresistance in topological insulator thin films, *Phys. Rev. B* 88, 041307(R) (2013)
46. A. Kawabata, Theory of negative magnetoresistance i. application to heavily doped semiconductors, *J. Phys. Soc. Jpn.* 49(2), 628 (1980)
47. Y. Kopelevich, J. H. S. Torres, R. R. da Silva, F. Mrowka, H. Kempa, and P. Esquinazi, Reentrant metallic behavior of graphite in the quantum limit, *Phys. Rev. Lett.* 90(15), 156402 (2003)
48. B. Fauqué, B. Vignolle, C. Proust, J. P. Issi, and K. Behnia, Electronic instability in bismuth far beyond the quantum limit, *New J. Phys.* 11(11), 113012 (2009)
49. Y. P. Li, Z. Wang, Y. H. Lu, X. J. Yang, Z. X. Shen, F. Sheng, C. Feng, Y. Zheng, and Z.-A. Xu, Negative magnetoresistance in topological semimetals of transition-metal dipnictides with non-trivial Z_2 indices, arXiv: 1603.04056 (2016)
50. B. Shen, X. Y. Deng, G. Kotliar, and N. Ni, Fermi surface topology and negative longitudinal magnetoresistance observed in centrosymmetric $NbAs_2$ semimetal, arXiv: 1602.01795 (2016)
51. Y. K. Luo, R. D. McDonald, P. F. S. Rosa, B. Scott, N. Wakeham, N. J. Ghimire, E. D. Bauer, J. D. Thompson, and F. Ronning, Anomalous magnetoresistance in $TaAs_2$, arXiv: 1601.05524 (2016)
52. Z. Wang, Y. P. Li, Y. H. Lu, Z. X. Shen, F. Sheng, C. M. Feng, Y. Zheng, and Z. A. Xu, Topological phase transition induced extreme magnetoresistance in $TaSb_2$, arXiv: 1603.01717 (2016)
53. V. K. Dugaev and D. E. Khmelnitskii, Magnetoresistance of metal films with low impurity concentration in a parallel magnetic field, *Sov. Phys. JETP* 59, 1038 (1984)
54. A. K. Mitchell and L. Fritz, Kondo effect in three-dimensional Dirac and Weyl systems, *Phys. Rev. B* 92, 121109(R) (2015)